Collisions of Highly Vibrationally Excited Pyrazine (E_{vib} = 37 900 cm^{-1}) with HOD: State-Resolved Probing of Strong and Weak Collisions

Daniel K. Havey,[†] Qingnan Liu,[†] Ziman Li,[†,‡] Michael Elioff,[‡] and Amy S. Mullin*[,†,‡]

Department of Chemistry and Biochemistry, University of Maryland, College Park, Maryland 20742, and Department of Chemistry and Biochemistry, Boston University, Boston, Massachusetts 02215

Received: July 30, 2007; In Final Form: October 5, 2007

This work presents state-resolved measurements of weak and strong collisions between HOD and highly vibrationally excited pyrazine (E_{vib} = 37 900 cm^{-1}). Transient IR absorption line profiles of HOD(000) rotational states that are populated in single collisions with pyrazine (E_{vib}) are fit using double-Gaussian functions to extract Doppler-broadened line widths and energy transfer rates for appearance and depletion populations. We recently reported the use of this new approach to determine collision rates for energy transfer (Havey, D. K.; Liu, Q.; Li, Z. M.; Elioff, M.; Fang, M.; Neudel, J.; Mullin, A. S. *J. Phys. Chem. A* **2007**, *111*, 2458−2460). Here we present a full description of transient measurements of weak collisions, along with rate constants and the full energy transfer distribution function for the vibrational-to-rotation/translation (V−RT) pathway. The low- and high-*J* populations of scattered HOD(000) are characterized by a single rotational distribution with T_{rot} = 430 ± 50 K. The average translational energy of the scattered HOD(000) increases modestly with rotational energy suggesting an impulsive energy transfer mechanism. The energy gain distribution $P(\Delta E)$ for HOD(000) shows that ∼99% of collisions have ΔE values less than 3000 cm^{-1}. These data yield a lower limit to the collision rate that is ∼70% larger than the calculated Lennard-Jones collision rate. These findings show that water is an efficient quencher due to a large collisional energy transfer cross section and not as a result of a large supercollision tail.

Introduction

Collisional quenching of high-energy molecules is of multidisciplinary significance. Atmospheric photochemistry is governed by the extent to which vibrationally excited[1−4] or electronically excited[5−9] chromophores are relaxed by collisions before undergoing chemical reactions. In high-temperature chemistry such as in the area of combustion, collisional relaxation of highly excited molecules competes directly with unimolecular decomposition.[10−14] Miller, Klippenstein, and coworkers have reported that average energy transfer values are usually adequate for simulating threshold reaction processes but that a more detailed description of the distribution of energy transfer is needed to understand bimolecular reactions occurring above deep potential wells.[15,16] A complete description of collisional relaxation requires an understanding of the dynamics of both strong and weak collisions, but until recently techniques to probe weak collisions directly have not been available. Recently we described a new approach that uses transient IR absorption to measure the outcome of weak collisions between highly vibrationally excited pyrazine and HOD.[17] Here we present a full description of this approach and compare the energy partitioning and energy transfer rates for weak and strong collisions. These experiments provide the first state-resolved glimpse at the dynamics of both strong and weak collisions the quench highly vibrationally excited molecules.

A number of approaches have been used to measure the collisional relaxation of highly excited molecules. First and second moments of the energy transfer distribution function have been obtained by monitoring population changes in highly excited molecules, using methods such as UV absorption (UVA),[18−21] IR fluorescence (IRF),[22−25] and kinetically controlled selective ionization (KSCI).[26−31] KCSI monitors the appearance of polyatomic donors in well-defined energy windows as they undergo collision quenching and directly yields an energy transfer distribution function. The dynamics of collisional energy transfer have been investigated by a number of techniques that monitor the appearance of product states. Vibrational energy gain in bath molecules has been probed using IRF[22−25] and FTIR emission.[32−34] High-resolution transient IR probing is a particularly useful approach for measuring energy gain distributions since the partitioning of exchanged energy among the vibrational, rotational, and translational degrees of freedom in the bath molecule is resolved.[17,35−42] This approach has been used for a number of donor/acceptor pairs to elucidate the dynamics of strong collisions which transfer large amounts of energy.[38,43−56] By focusing on the appearance of bath states that are not thermally populated prior to collisions with the hot donor molecule, transient absorption signals for strong collisions correspond purely to population gains due to collisional excitation. Probing strong collisions in this way is straightforward in principle but can be challenging due to the low probability of strong collisions. Weak collisions, on the other hand, involve relatively small energy exchanges that lead to population changes that occur within the states that are initially populated thermally and make up the bulk of collisional energy transfer. Despite the prevalence of weak collisions, little is known about their dynamics.[26−31]

A number of factors potentially complicate state-resolved energy gain measurements for the low-energy bath states that are involved in weak collisions. Depletion of relatively large initial thermal populations may obscure energy gain measure-

[†] University of Maryland.
[‡] Formerly at Boston University.

10.1021/jp076023i CCC: $37.00
Published on Web 12/04/2007

ments, large atmospheric absorption can interfere with probe laser intensity, and since absorption is sensitive to population differences, collisional energy transfer that populates the upper state of the probe transition can artificially reduce observed energy gain signals. For HOD, we have been able to overcome these challenges and have measured for the first time the state-resolved energy gain profiles for the low-energy rotational states that correspond to the weak collisions of a highly vibrationally excited aromatic molecule with water.[17] These results provide a simultaneous picture of the dynamics involved in weak and strong collisions for relaxing highly excited molecules.

Here the nascent product state distributions for low- and high-J rotational states of HOD in its ground vibrationless state (000) are reported that result from collisions of vibrationally hot pyrazine ($E_{vib} = 37\,900$ cm^{-1}). The appearance of HOD product rotational states is probed using high-resolution transient IR absorption near $\lambda = 2.7$ μm. The nascent translational energy distributions for individual product rotational states are determined from transient Doppler-broadened line shapes. We find that the scattered HOD molecules in both low- and high-J states fit to a single rotational distribution that is relatively cold and that the translational energy of the scattered molecules does not depend strongly on the HOD rotational angular momentum for $J = 2-12$. The energy transfer rates for individual product states are measured directly and have an integrated rate that is nearly twice the Lennard-Jones collision rate indicating the energy transfer between hot pyrazine and HOD occurs on essentially every collision.

Experimental Methods

The present study was performed using an IR transient absorption spectrometer containing a pulsed Nd:YAG pump laser and a continuous F-center probe laser. This apparatus has been described in detail previously.[38] The KCl:Li and RbCl:Li crystals (II and III, respectively) in the F-center laser were pumped by less than 1.5 W of all lines red light from a Kr^+ laser. This configuration was sufficient for generating probe light for HOD(001 ← 000) rovibrational transitions near $\lambda = 2.57-2.7$ μm ($\bar{\nu} \sim 3900-3700$ cm^{-1}). Highly vibrationally excited pyrazine in the ground electronic state was prepared using the fourth harmonic ($\lambda = 266$ nm) of the Nd:YAG pump laser. Pyrazine is electronically excited by 266 nm excitation but undergoes rapid radiationless decay to its electronic ground state while remaining in a relatively long-lived vibrationally excited state ($\tau \sim 70$ μs).[57,58] One pulse/s from the 10 Hz pump laser was allowed to interact with pyrazine, and the intensity was kept lower than 4.2 MW/cm^2 to minimize multiphoton absorption by the donor.

Single-mode operation of the F-center probe laser was obtained using an intracavity etalon that was locked to a single-cavity mode. Continuous frequency scanning was obtained using active feedback control.[59] To scan, two CaF_2 galvo plates were rotated to change the laser's cavity length. Simultaneously, the spacing of an intracavity etalon was scanned to maintain single-mode operation while the cavity length was tuned. This method provides single-mode scanning across a frequency range of $\sim$0.07 cm^{-1}. The scanning rate for this work is 0.0578 cm^{-1}/1 V ramp applied to galvo plates.

Both the pump and probe light were propagated collinearly through a 250 cm Pyrex collision cell. A 1:2 mixture of pyrazine and H_2O/HOD/D_2O vapor at a total pressure of $\sim$30 mTorr at 300 K flowed through the collision cell with a mean collision time of $\tau \sim 3$ μs. About 15% of the pyrazine molecules were optically excited under these conditions. A 1:1 mixture by volume of H_2O and D_2O yields an equilibrium mixture of HOD/D_2O/H_2O with a 2:1:1 concentration ratio.[60] The pressure of HOD was measured spectroscopically using known absorption intensities of rovibrational transitions within the (001 ← 000) absorption. The gas samples were prepared by controlling flow of the vapor pressures over H_2O/HOD/D_2O and pyrazine liquids. Research grade pyrazine (Aldrich, 99+%) was used after undergoing several freeze/pump/thaw cycles to remove atmospheric gases. H_2O and D_2O (Cambridge Isotope Laboratories, 99.9%) were fractionally distilled and sealed together in a vacuum flask at 100 °C. Both samples were maintained in vacuum flasks connected to a vacuum line with pressure less than 1 mTorr.

Transient absorption traces $T(t)$ for individual HOD states were collected for up to 5 μs following the Nd:YAG laser pulse. Linear absorption signals between 0.5 and 1.5 μs were averaged to give a measurement of $T(t)$ in the single-collision regime at $t = 1$ μs. Simultaneously, a background signal of 10% intensity of the F-center beam was collected in order to account for time-dependent power fluctuations of the probe laser.

Results and Discussion

We have measured the full distribution of HOD(000) molecules that are scattered in single collisions from highly vibrationally excited pyrazine molecules using high-resolution transient absorption probing at $\lambda = 2.7$ μm. The outcome of weak and strong collisions was measured from Doppler-broadened line profiles for appearance of individual HOD(000) product states. These data offer the first experimental comparison of the dynamics of weak and strong collisions that quench highly vibrationally excited molecules. Energy transfer rates for the full product state distribution provide a direct measure of the collision rate. Here we describe our approach to extract information about the weak collisions and present our results.

Transient Absorption of HOD(000). Collisions between vibrationally hot pyrazine, Pyz(E_{vib}), and HOD lead to energy changes in both collision partners (eq 1)

$$\mathrm{Pyz}(E_{vib} = 37\,900\ \mathrm{cm}^{-1}) + \mathrm{HOD}(300\ \mathrm{K}) \xrightarrow{k_{app}^{J}} \mathrm{Pyz}(E_{vib}') + \mathrm{HOD}(000, J_{Ka,Kc}, V) \quad (1)$$

The appearance of scattered HOD(000) molecules is monitored with high-resolution transient IR absorption. The vibrational energy in pyrazine prior to collisions is $E_{vib} = 37\,900$ cm^{-1}. After collisions, the final pyrazine vibrational energy is E_{vib}', which can either be larger or smaller than E_{vib} depending on whether collisions quench or impart energy to pyrazine. The appearance of an individual rotational state of HOD(000) occurs with a rate constant k_{app}^{J} that is indexed by the final HOD state. In eq 1, (000) represents the ground vibrationless state of HOD, J is the total angular momentum quantum number, and Ka and Kc are projections of the angular momentum on the A and C axes, respectively.

High-resolution IR probing is used to monitor the quantum state-resolved population changes in HOD(000) resulting from eq 1. The probe transitions involve excitation of the OH stretching mode of HOD near $\lambda = 2.7$ μm.

$$\mathrm{HOD}(000, J_{Ka,Kc}, V) + h\nu(\lambda \sim 2.7\ \mu\mathrm{m}) \rightarrow \mathrm{HOD}(001, J'_{Ka',Kc'}, V) \quad (2)$$

In eq 2, (001) represents one quantum in the OH stretch and V is the component of the velocity vector parallel to the IR

propagation axis. Nascent HOD(000) populations resulting from single collisions between pyrazine and HOD are obtained from measurements at $t = 1$ μs following the UV pulse. The 1 μs measurement time is well before the average collision time of $\tau_{col} \sim 3$ μs.

Weak collisions between pyrazine(E_{vib}) and HOD involve small changes in rotational angular momentum and induce population changes in the low-J states of HOD. A major challenge of measuring energy gain in low-J states is the need to determine small population changes for states that have substantial initial thermal population. Here, we use the HOD-(000, $2_{2,0}$) state as an example to show how transient populations are extracted from the thermal background. The $2_{2,0}$ state has an energy of $E_{rot} = 109$ cm^{-1} and is thermally populated at 300 K. The IR probe transition for this state, HOD(001, $2_{2,1}$) ← HOD(000, $2_{2,0}$), monitors population changes in the $2_{2,0}$ state. The collision-induced population changes for this state can result from appearance of scattered molecules (eq 1) and depletion of initial population (eq 3).

$$\mathrm{Pyz}(E_{vib}) + \mathrm{HOD}(000, 2_{2,0}) \xrightarrow{k^J_{app}} \mathrm{Pyz}(E_{vib}') + \mathrm{HOD}(\text{any other state}) \quad (3)$$

The depletion of initial population due to collisions occurs with a rate constant k^J_{dep}. In addition, collisions with hot pyrazine can directly populate the upper state of the probe transition directly (eq 4).

$$\mathrm{Pyz}(E_{vib}) + \mathrm{HOD}(300\ \mathrm{K}) \rightarrow \mathrm{Pyz}(E_{vib} - \Delta E) + \mathrm{HOD}(001, 2_{2,1}) \quad (4)$$

The collision-induced appearance of the HOD(001, J_{KaKc}) states was investigated separately using 002 ← 001 probe transitions. No transient absorption signals were observed, and eq 4 can be neglected here. The collision-induced population changes in low-J HOD states with large initial thermal populations are completely described by eqs 1 and 3. For high-J HOD states with negligible thermal populations, the transient signals are described solely by eq 1. By characterizing the components of the IR signals from appearance and depletion (where necessary), the nascent energy partitioning of the scattered molecules is obtained.

Figure 1 shows transient signals for two different HOD states with the IR probe tuned to the center of the probe transition. The transient absorption for the $2_{2,0}$ state is shown in Figure 1a. The rate of population loss (via eq 3) at line center is greater than that of appearance, so the transient signal shows net depletion for this state. The $12_{2,10}$ state has a rotational energy of $E_{rot} = 1331$ cm^{-1}, and its transient signal at line center shows only appearance of population, as seen in Figure 1b. HOD states with $E_{rot} > 500$ cm^{-1} show only appearance. Collisional energy transfer involving HOD rotational states with $E_{rot} < 500$ cm^{-1} and 1020 cm^{-1} $< E_{rot} <$ 1340 cm^{-1} are reported in this paper. Transient signals for states with 500 cm^{-1} $< E_{rot} <$ 1020 cm^{-1} and $E_{rot} >$ 1340 cm^{-1} had low signal-to-noise ratios, as described in the next section.

Analysis of Weak Collision Line Profiles. Transient absorption profiles for weak collisions are obtained by collecting transient absorption signals as a function of IR wavelength at $t = 1$ μs after the UV pulse. Figure 2 shows transient line profiles for HOD states with energies $E_{rot} = 109-474$ cm^{-1}. At ν_0, the center of each profile, there is a strong negative-going signal corresponding to depletion and a second positive-going component in the wings at approximately $\nu_0 \pm 0.0125$ cm^{-1}. The positive-going component for the low-J states corresponds to HOD molecules scattering into the probe state as a result of weak collisions.

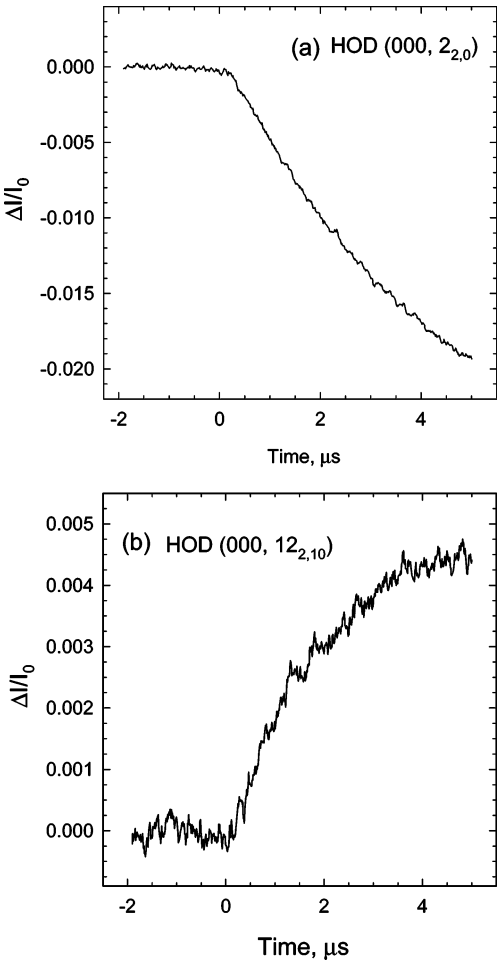

Figure 1. Fractional IR absorption of HOD(000) following collisions of highly excited pyrazine ($E_{vib} = 37\,900$ cm^{-1}) with HOD measured at ν_0 as a function of time following UV excitation of pyrazine. The collision cell pressure is ~30 mTorr at 300 K, and the gas kinetic collision time is approximately 3 μs. Panel a shows depletion of HOD-(000, $2_{2,0}$) with $E_{rot} = 109$ cm^{-1}, and panel b shows appearance of HOD(000, $12_{2,10}$) with $E_{rot} = 1331$ cm^{-1}.

Prior to quenching collisions, there is an isotropic distribution of molecules in our experiments. Doppler-broadened line profiles for isotropic ensembles are characterized by a Gaussian distribution with respect to IR frequency ν. Separate appearance and depletion populations for each low-J state are determined by performing nonlinear least-squares analysis with a double-Gaussian function $F(\nu)$ (eq 5). The fit includes six parameters for the appearance and depletion line shapes.

$$F(\nu) = F_0 + I_{app} \exp\left[-4 \ln 2\left(\frac{\nu - \nu_0}{\Delta\nu_{app}}\right)^2\right] - I_{dep} \exp\left[-4 \ln 2\left(\frac{\nu - \nu_0}{\Delta\nu_{dep}}\right)^2\right] \quad (5)$$

Here, F_0 adjusts for small offsets in the baseline, ν_0 is the center frequency of the transition, I_{app} and I_{dep} correspond to the intensities for appearance and depletion, respectively, and the full width at half-maximum (fwhm) line widths for the appearance and depletion populations are $\Delta\nu_{app}$ and $\Delta\nu_{dep}$, respectively. The line widths correspond to the lab-frame translational temperatures of the HOD velocity distributions.

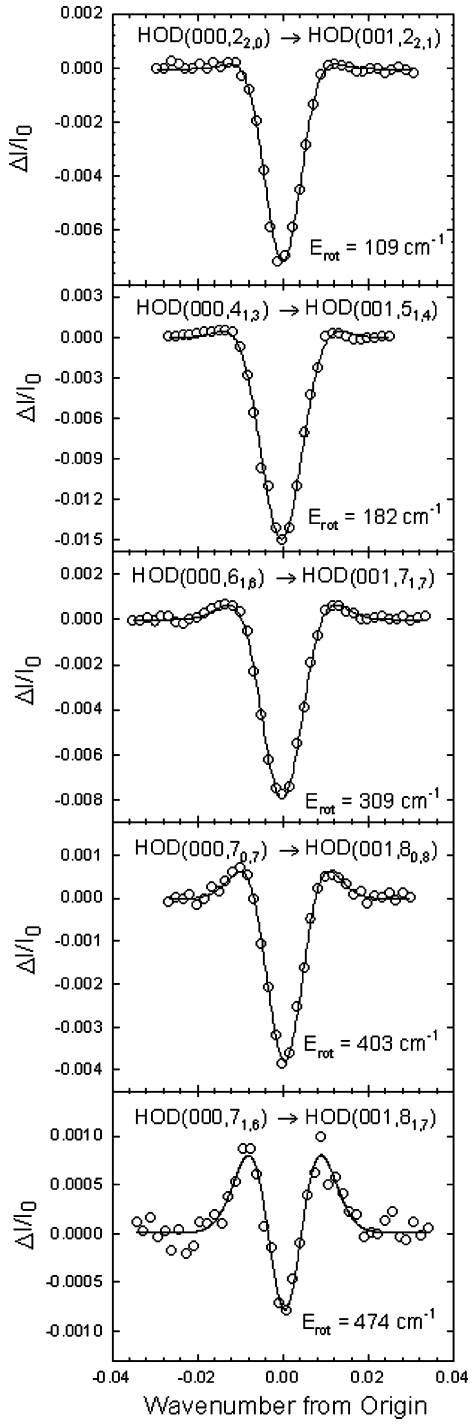

Figure 2. Transient absorption line shapes for HOD(000) low-J rotational states with $E_{rot} < 500$ cm^{-1} collected at 1 μs following UV excitation of pyrazine. Transient absorption data (open circles) show depletion at the transition origin and appearance in the Doppler-broadened wings. The data are fit to a double-Gaussian function (eq 5), shown as solid lines.

The fitting results of the low-J states are shown in Figure 2 and listed in Table 1. The depletion line widths $\Delta\nu_{dep}$ have values of $T_{dep} \sim 315-350$ K which are very close to the initial ambient cell temperature of 300 K. Our experimental resolution is sufficient to measure HOD velocity distributions with temperatures as low as $T \sim 100 \pm 50$ K. Our T_{dep} measurements show that the initial velocity distribution of the HOD molecules that undergo collisional energy transfer is essentially the same as the thermal velocity distribution. This suggests that there is no preference for energy transfer into the HOD(000) state due to a subset of the initial velocity distribution.

Obtaining unique fitting results for the double-Gaussian functions requires two conditions to be satisfied. First, we find that experimental data for a low-J state ($E_{rot} < 250$ cm^{-1}) that is dominated by depletion must have a signal-to-noise ratio based on the signal level at line center relative to baseline greater than about 15:1. For HOD states with rotational energies between 250 cm^{-1} < E_{rot} < 500 cm^{-1} the signal-to-noise ratio must be at least 3:1 at the peak absorption of the wings and line center. Second, it is useful to guide the intensity and line width parameters (I_{app}, $\Delta\nu_{app}$, I_{dep}, $\Delta\nu_{dep}$) by a reasonable set of physical constraints. The intensity parameters were limited to be positive but less than 0.05. This value sets an upper limit to the rate constant of the hard sphere collision rate for appearance or depletion of a single quantum state. This is at least a factor of 10 larger than the energy transfer rates expected for individual low-J states. The line width parameters for appearance and depletion were constrained using $0 < \Delta\nu_{dep} < \Delta\nu_{app} < 0.019$ cm^{-1}, where the upper limit is based on twice the average translational energy observed for the high-J HOD measurements that are described below. Fitting results were checked to ensure that each parameter had an optimum converged value. Multiple series of five-parameter fits confirmed that the final value for each parameter minimized the sum of the residuals from the least-squares analysis.

Translational Energy Imparted in Weak Collisions. The translational energy distributions from weak pyrazine/HOD collisions were determined from Doppler-broadened line widths for a number of low-J states of HOD. The appearance profiles for the states shown in Figure 2 are broadened relative to 300 K and have a range of lab-frame translational temperatures from $T_{app} = 493 \pm 74$ to 578 ± 87 K. Converting to the center-of-mass frame[38] yields relative translational temperatures of $T_{rel} = 539 \pm 81$ to 645 ± 97 K. The relative translational temperature accounts for the velocities of both scattered collision partners. The average change in translational energy due to collisions is estimated using $\langle\Delta E_{rel}\rangle = (3/2)k_B(T_{rel} - T_0)$ with $T_0 = 300$ K based on our depletion line width measurements. The average translational energy imparted through weak collisions for the low-J states of HOD is $\langle\Delta E_{rel}\rangle \sim 250-350$ cm^{-1}, as listed in Table 1.

Translational Energy Imparted in Strong Collisions. The translational energy distributions from strong pyrazine/HOD collisions were determined from Doppler-broadened line profiles for high-J states of HOD. The transient line shape for the HOD-(000,10$_{3,7}$) state with $E_{rot} = 1024$ cm^{-1} is shown in Figure 3. The experimental data are fit using eq 5 by setting $I_{dep} = 0$. The appearance line width for this state is $\Delta\nu_{app} = 0.0159 \pm 0.0010$ cm^{-1}, corresponding to a lab-frame translational temperature of $T_{app} = 697 \pm 105$ K. The relative translational temperature is $T_{rel} = 792 \pm 119$ K, and the average change in relative translational energy is $\langle\Delta E_{rel}\rangle \sim 515 \pm 65$ cm^{-1}. Translational energy increases for the high-J HOD states have a range of values of $\langle\Delta E_{rel}\rangle = 384-515$ cm^{-1}, as listed in Table 2 .

Scattering data for low- and high-J states of HOD allow us for the first time to compare the translational energy from weak and strong collisions of highly vibrationally excited molecules. The relative translational energy of the scattered molecules is plotted in Figure 4 as a function of final HOD rotational state where it is seen that the relative translational energy increases slightly as a function of HOD rotational energy. HOD states with low rotational energies are scattered with $\langle E_{rel}\rangle \sim 600$ cm^{-1},

TABLE 1: Translational Energy Profiles of HOD(000, $J_{Ka,Kc}$) Low-J States Resulting from Collisions with Highly Vibrationally Excited Pyrazine (E_{vib} = 37 900 cm^{-1})

$J_{Ka,Kc}$	ν_0, cm^{-1}	E_{rot}, cm^{-1}	$\Delta\nu_{app}$, cm^{-1} [a]	T_{app}, K[b]	T_{rel}, K[c]	$\langle\Delta E_{rel}\rangle$, cm^{-1} [d]	$\Delta\nu_{dep}$, cm^{-1} [e]	T_{dep}, K[f]
$2_{2,0}$	3702.904	109.269	0.0136	500 ± 75	548 ± 82	261 ± 39	0.0108	315 ± 47
$4_{1,3}$	3787.510	182.983	0.0146	550 ± 83	610 ± 92	325 ± 49	0.0113	330 ± 49
$6_{1,6}$	3798.189	308.615	0.0150	578 ± 87	645 ± 97	362 ± 54	0.0113	328 ± 49
$7_{0,7}$	3810.595	403.161	0.0139	493 ± 74	539 ± 81	251 ± 38	0.0117	349 ± 52
$7_{1,6}$	3826.241	473.918	0.0141	503 ± 75	552 ± 83	265 ± 40	0.0112	317 ± 48

[a] $\Delta\nu_{app}$ is the full width at half-maximum (fwhm) line width from transient absorption appearance line profiles (ref 63) measured at 1 μs following 266 nm excitation of pyrazine. Transient line profiles for HOD(000) states with 100 cm^{-1} < E_{rot} < 500 cm^{-1} are fit to a double-Gaussian function (eq 5 in text). Each $\Delta\nu_{app}$ has an uncertainty of ±0.001 cm^{-1}. Experimental accuracy for line shapes was determined by measuring multiple 298 K line widths of a CO_2 ($00^00 \rightarrow 10^01$, P40) transition which agreed with the known value to within 0.0007 cm^{-1}. [b] Lab-frame translational temperatures for appearance of HOD(000, $J_{Ka,Kc}$) are determined using $T_{app} = (mc^2/(8k_B \ln 2))(\Delta\nu_{app}/\nu_0)^2$ where m is the mass of HOD, c is the speed of light, k_B is Boltzmann's constant, ν_0 is the center frequency of the probe transition, and $\Delta\nu_{app}$ is the experimentally measured fwhm line width. [c] Center-of-mass frame translational temperatures T_{rel} for an isotropic distribution are found using $T_{rel} = T_{app} + (T_{app} - T_0)(m_{HOD}/m_{pyrazine})$ where T_0 = 298 K. m_{HOD} and $m_{pyrazine}$ are the masses of HOD and pyrazine (ref 38). [d] The average relative translational energy change $\langle\Delta E_{rel}\rangle$ is determined from $\langle\Delta E_{rel}\rangle = {}^3/_2 k_B(T_{rel} - T_0)$ where T_0 = 298 K. [e] $\Delta\nu_{dep}$ is fwhm Doppler-broadened line width for population depletion from HOD states with 100 cm^{-1} < E_{rot} < 500 cm^{-1}. [f] Lab-frame translational temperatures T_{dep} for depletion of initial HOD(000, $J_{Ka,Kc}$) are determined similarly to T_{app} in footnote *b* above using $\Delta\nu_{dep}$.

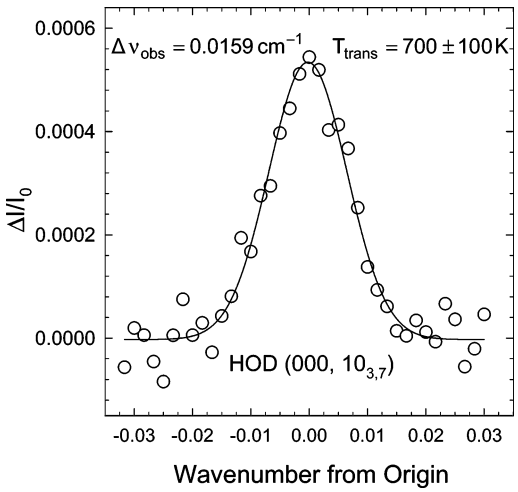

Figure 3. Transient absorption line shape for HOD(000, $10_{3,7}$) collected at 1 μs following UV excitation of pyrazine. The data (open circles) are fit to a single-Gaussian function (eq 5 with $I_{dep} = 0$) which is shown as a solid line.

whereas high-energy states have $\langle E_{rel}\rangle \sim 750$ cm^{-1}. Impulsive collisions are expected to import larger recoil velocities when the collisions involve large changes in angular momentum. Therefore, the amount of energy released in the form of translation is sensitive to the rotational energy spacing of the bath molecule. As the rotational energy spacing increases, the energy gap is taken up by fewer ΔJ quanta and smaller recoil velocities. HOD has relatively large rotational spacing (the rotational constants of HOD are A = 23.4 cm^{-1}, B = 9.1 cm^{-1}, and C = 6.4 cm^{-1}) and is scattered from vibrationally hot pyrazine with relatively small amounts of translational energy. The J-dependent increase in $\langle E_{rel}\rangle$ for HOD collisions is relatively small but is consistent with an impulsive energy transfer mechanism where the strong collisions lead to somewhat larger recoil velocities than the weak collisions. The J-dependent velocity increases in pyrazine collisions with CO_2 are much more pronounced and include J states up to J = 80.[44,49,61] Of course, CO_2 has more closely spaced rotational states (B = 0.394 cm^{-1}) than HOD. The J-dependent HOD translational energy gains are comparable to those seen for H_2O since the rotational spacing in H_2O is only slightly larger than for HOD.[38]

Rotational Energy of Scattered HOD. The rotational distribution of scattered HOD molecules was determined for states with E_{rot} from 0 to 1400 cm^{-1}. The populations of both low- and high-J states of scattered HOD(000) are shown in the semilog plot of Figure 5. The populations were determined from fractional absorption measurements at 1 μs and include contributions from Doppler-broadened transient line widths. The rotational distribution of scattered HOD(000) molecules is characterized by a single-exponential distribution with a rotational temperature of T_{rot} = 430 ± 50 K. When only the high-J states of HOD are fit, the result is within 3% of this value. This indicates that vibrational-to-rotation/translation (V−RT) energy transfer from pyrazine to HOD has cross sections that are consistent with energy gap control. It is interesting that the rotational temperature of scattered HOD is substantially lower than that reported previously for pyrazine/H_2O collisions (where $T_{rot} \sim$ 920 K for the scattered H_2O)[38] and for pyrazine/CO_2 collisions ($T_{rot} \sim$ 1200 K for CO_2).[61] This suggests that rotational state structure and possibly electrostatic and dynamics factors contribute to the extent of rotational energy gain in the quenching of high-energy molecules. These issues will be explored more fully when a more complete comparison of H_2O and HOD as quenchers is presented in a future paper.

Energy Transfer Rate Constants for Collisions of Pyrazine (E_{vib}) and HOD. Rate constants for appearance of both low- and high-J product states of HOD from collisions with highly vibrationally excited pyrazine provide an excellent measure of the overall collision rate for V−RT energy transfer. As described earlier, population changes for individual HOD(000) states result from a combination of appearance (eq 1) and depletion (eq 3). The distribution of HOD molecules prior to energy transfer has a temperature T_0 that is simply the equilibrium distribution of HOD molecules prior to collisions with vibrationally hot pyrazine. Our depletion line widths show that T_0 is very close to 300 K. The HOD molecules that are scattered by collisions into a particular J-state are a subset of the total HOD concentration and have a nascent energy distribution that is characterized by T_{sub}. The appearance rate of an HOD product state is quantified by eq 6 and has a rate constant k_{app}^J.

$$\frac{d[HOD(J_{KaKc}, T_{sub})]}{dt} = k_{app}^J[Pyz(E_{vib})][HOD(T_0)] \quad (6)$$

Appearance rate constants were determined using the method of initial rates. The number densities of Pyz(E_{vib}) and HOD are essentially constant immediately following the UV excitation of pyrazine. Transient absorption signals, such as the one shown in Figure 1b, are linear for the first few microseconds following UV excitation, in agreement with this kinetic model. Initial concentrations, $[Pyz(E_{vib})]_0$ and $[HOD]_0$ were determined

TABLE 2: Translational Energy Gain in HOD(000, $J_{Ka,Kc}$) High-J States Following Collisions with Highly Vibrationally Excited Pyrazine (E_{vib} = 37 900 cm^{-1})

$J_{Ka,Kc}$	ν_0, cm^{-1}	E_{rot}, cm^{-1}	$\Delta\nu_{app}$, cm^{-1} [a]	T_{app}, K[b]	T_{rel}, K[c]	$\langle\Delta E_{rel}\rangle$, cm^{-1} [d]
$10_{3,7}$	3664.909	1024.568	0.0159	697 ± 105	792 ± 119	515 ± 65
$11_{3,8}$	3739.334	1164.509	0.0151	604 ± 91	677 ± 102	395 ± 52
$12_{1,11}$	3876.128	1220.027	0.0157	608 ± 91	682 ± 102	400 ± 51
$12_{2,10}$	3893.025	1331.216	0.0156	595 ± 89	666 ± 100	384 ± 49

[a] $\Delta\nu_{app}$ is the fwhm line width from transient absorption appearance line shapes measured 1 μs following UV excitation of pyrazine. For HOD states with 1024 < E_{rot} < 1332 cm^{-1}, transient absorption line shapes are fit to a single-Gaussian function using eq 5 with $C = 0$. Each $\Delta\nu_{app}$ is the average of at least three measurements and has an uncertainty of ±0.001 cm^{-1}. [b] Lab-frame translational temperature for appearance of scattered HOD(000, $J_{Ka,Kc}$). [c] T_{rel} is the center-of-mass frame translational temperature. [d] $\langle\Delta E_{rel}\rangle = {}^3/_2 k_B(T_{rel} - T_0)$ is the average change in relative translational energy.

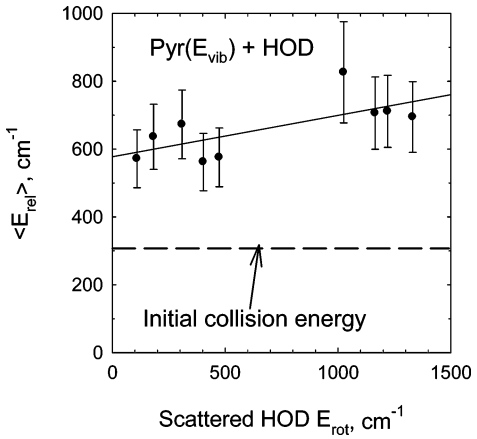

Figure 4. Average center-of-mass translational energies $\langle E_{rel}\rangle$ vs HOD-(000) E_{rot}. $\langle E_{rel}\rangle$ increases slightly as a function of HOD rotational energy for E_{rot} = 0−1500 cm^{-1}.

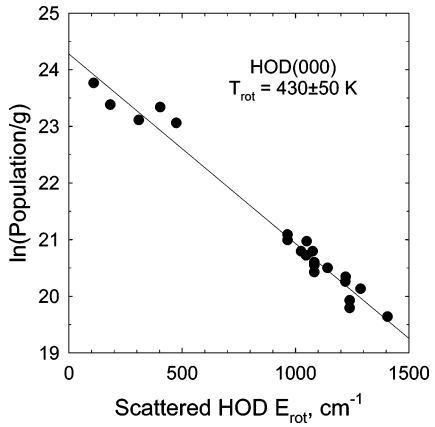

Figure 5. Nascent distribution of HOD(000) rotational states (filled circles) has a temperature T_{rot} = 430 ± 50 K.

spectroscopically using UV and IR absorption, respectively. Rate constants for the high-J states of HOD were determined directly using eq 6 and the peak intensity of the Doppler-broadened transient line profiles, shown in Figure 3 and Table 2. Appearance rate constants for the low-J states were determined using eq 6, with the IR intensities for appearance based on fitting the Doppler-broadened line profiles with a double-Gaussian function (eq 5).

Values of k^J_{app} are listed in Table 3 for HOD(000). The total energy transfer rate for the V−RT pathway is determined by summing over all product states. Appearance rate constants for the full distribution of HOD(000) were determined from the measured appearance rates (Table 3) and the nascent rotational temperature (T_{rot} = 430 ± 50 K, Figure 5). The integrated rate for appearance of HOD(000) with energies between E_{rot} = 0 and 2300 cm^{-1} is $k_{int} = 1.02 \pm 0.30 \times 10^{-9}$ cm^3 molecule^{-1} s^{-1}. Most of the energy transfer scatters HOD into rotational states with E_{rot} < 1000 cm^{-1}. Specifically, 95% of k_{int} is obtained by summing over states with E_{rot} = 0−1000 cm^{-1}.

These data also an opportunity to compare the energy transfer rate with collision rates from commonly used models. By measuring the energy gain rates and distributions for both weak and strong collisions, we account for all collisions that undergo V−RT energy transfer. These data provide a direct experimental measure of the lower limit to the actual collision rate between highly excited pyrazine and HOD. The integrated rate for V−RT energy transfer, $k_{int} = 1.02 \pm 0.30 \times 10^{-9}$ cm^3 molecule^{-1} s^{-1}, is larger than the hard sphere collision rate by a factor of 3 ($k^{HS}_{col} = 3.2 \times 10^{-10}$ cm^3 molecule^{-1} s^{-1}) and the Lennard-Jones collision rate by a factor of 1.7 ($k^{LJ}_{col} = 6.3 \times 10^{-10}$ cm^3 molecule^{-1} s^{-1}) The Lennard-Jones collision rate was calculated using σ = 3.96 Å and ϵ = 313 cm^{-1} for pyrazine/HOD.[62] Thus, energy transfer occurs on virtually every collision between highly excited pyrazine and HOD. It is interesting that the collision rates based on both hard sphere and Lennard-Jones potentials underestimate the actual collision frequency.[17] It is not clear at the present time whether this discrepancy is due to inadequacy of the Lennard-Jones collision model in describing molecular collisions or if the presence of large amounts of internal energy in the vibrationally excited molecule actually enhances the collision cross section. It would be interesting to know how k_{int} depends on the identity of the collision partners and energy of the highly excited molecule. These questions will be addressed in future studies.

The total collision rate accounts for the outcome of all collisions, including vibration to vibration (V−V) and reactive pathways. Here we have characterized the full HOD product distribution for the V−RT pathway. Collisions of hot pyrazine that lead to vibrational excitation of H_2O have been observed only for the ν_2 bending mode of H_2O. This pathway occur much less often than rotational and translational excitation of the (000) state[53] with an integrated rate for vibrational energy gain that is only about 5% of that for V−RT energy gain of the H_2O-(000) state. Additionally, no reactive pathways that produce HOD have been observed in our studies from a mixture of vibrationally hot pyrazine-h_4 and D_2O. Based on these findings, we conclude that the V−RT pathway is the dominant means by which vibrationally hot pyrazine is quenched in HOD, accounting for ∼95% of collisional energy transfer events.

Energy Transfer Probability Distribution $P(\Delta E)$ for HOD Energy Gain. In this section, the transient HOD data is used to determine the energy transfer distribution function for pyrazine/HOD collisions. The HOD state-resolved energy distributions account for all energy in the scattered HOD(000) molecules as well as the translational energy of the scattered pyrazine. The probability for energy gain into a single HOD product state is determined from the appearance rate for that state divided by the Lennard-Jones collision rate, that is $P_J = k_{app}/k^{LJ}_{col}$. Each final HOD(000) rotational state has a transla-

TABLE 3: Appearance Rates of HOD(000, $J_{Ka,Kc}$) from the Process Pyrazine (E_{vib} = 37 900 cm^{-1}) + HOD $\xrightarrow{k^J_{app}}$ Pyrazine (E'_{vib}) + HOD(000, $J_{Ka,Kc}$)

J_{KaKc}	ν_0, cm^{-1}	E_{rot}, cm^{-1} [a]	k^J_{app}, 10^{-12} cm^3 molecule^{-1} s^{-1} [b]
$2_{2,0}$	3702.904	109.269	13.8 ± 4.1
$4_{1,3}$	3787.510	182.984	19.6 ± 5.9
$6_{1,6}$	3798.189	308.616	18.8 ± 5.6
$7_{0,7}$	3810.595	403.162	15.9 ± 4.8
$7_{1,6}$	3826.241	473.918	12.6 ± 3.6
$10_{2,8}$	3757.296	964.851	3.6 ± 1.1
$10_{3,7}$	3879.275	1024.569	2.9 ± 0.9
$11_{1,10}$	3866.368	1046.474	3.0 ± 0.9
$11_{2,10}$	3864.729	1049.125	3.0 ± 0.9
$12_{1,12}$	3864.216	1075.763	2.9 ± 0.9
$9_{5,5}$	3835.743	1082.785	2.2 ± 0.6
$9_{5,6}$	3836.070	1082.887	2.2 ± 0.6
$11_{2,9}$	3884.079	1141.692	2.2 ± 0.6
$12_{1,11}$	3876.128	1220.029	1.9 ± 0.6
$12_{2,11}$	3875.159	1221.537	1.9 ± 0.6
$10_{5,6}$	3850.937	1238.795	1.4 ± 0.4
$10_{5,5}$	3851.730	1239.089	1.4 ± 0.4
$11_{4,7}$	3884.345	1287.239	1.4 ± 0.4
$13_{1,12}$	3885.844	1405.818	1.1 ± 0.3
all states			k_{int} = (1.02 ± 0.30) × 10^{-9} cm^3 molecule^{-1} s^{-1} [c]

[a] The energy in cm^{-1} of the $J_{Ka,Kc}$ rotational states of HOD(000) from the HITRAN spectral database. [b] The appearance rate k^J_{app} is defined by eq 1 in the text. HOD population measurements include contributions from Doppler-broadened line widths shown in Tables 1 and 2. For high-J states where line widths were not measured, the average high-J line width of $\langle\Delta\nu_{obs}\rangle \sim 0.0156$ cm^{-1} was used. [c] The integrated energy transfer rate constant k_{int} for energy gain in HOD(000) is determined by summing over all values of k^J_{app} from E_{rot} = 0−2300 cm^{-1} (Figure 6).

tional energy distribution that is described by the temperature T_{rel}, as listed in Tables 1 and 2. A J-specific distribution function $P_J(\Delta E)$ is determined from the appearance rate and the relative translational temperature T_{rel} for that state, given by eq 7.[50,63]

$$P_J(\Delta E)\,\mathrm{d}\Delta E = \frac{4\pi}{\mu}\frac{k_{app}}{k_{LJ}}g_f\left(\frac{\mu}{2\pi k_B T_{rel}}\right)^{3/2}\exp\left(-\frac{\mu g_f^2}{2k_B T_{rel}}\right)\mathrm{d}\Delta E \quad (7)$$

Here, k_B is Boltzmann's constant, μ is the reduced mass, and g_f is the final velocity. The energy change ΔE is based on average initial rotational and translational energies at 300 K. Our data show only small variations in T_{rel} for the HOD states probed (Tables 1 and 2). The average value of T_{rel} was used in eq 7. The overall energy transfer distribution function $P(\Delta E)$ for energy gain of the V−RT pathway is obtained directly by summing over the J-state indexed translational energy distributions, such that $P(\Delta E) = \sum P_J(\Delta E)$. This distribution accounts for all transferred energy in the V−RT pathway with the exception of changes in the rotational energy of pyrazine. Figure 7 shows the $P(\Delta E)$ distribution function for V−RT energy transfer from collisions of pyrazine (E_{vib}) and HOD.

A complete description of energy transfer for a particular pathway requires knowledge of the vibrational, rotational, and translational energy changes for both donor and acceptor molecules. This entails knowledge of 12 parameters for each collision. With the exception of donor vibrational energy which is determined by the UV photon energy, all degrees of freedom are in equilibrium at 300 K prior to collisional energy transfer. State-resolved probing of energy gain in HOD in the single-collision regime completely characterizes the energy partitioning in HOD as well as the translational energy of the scattered pyrazine. We have therefore accounted for 10 of the 12 parameters with the remaining two quantities being the vibration and rotation of pyrazine following collisions. Since these are the only missing parameters, it should be possible using reasonable assumptions to extract detailed information from $P(\Delta E)$. At this time, it is not entirely clear how best to relate $P(\Delta E)$ to the entire energy transfer distribution function. This issue is a subject of ongoing investigation.

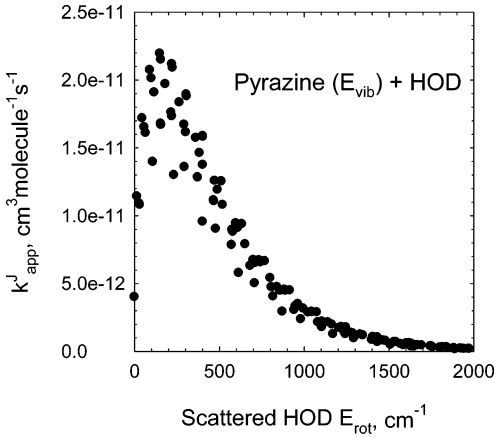

Figure 6. Rate constants k^J_{app} for appearance of HOD(000) following collisions with vibrationally hot pyrazine, based on the rate constants in Table 3 and the data in Figure 7. Values of k^J_{app} for HOD include a nuclear spin degeneracy of g_{ns} = 6 and a rotational degeneracy of $g_{rot} = 2J + 1$. The relatively low rotational temperature of HOD compresses the population to lower states. The integrated rate constant for appearance is larger than the Lennard-Jones collision rate constant by a factor of 1.7, meaning that energy transfer from hot pyrazine to HOD-(000) occurs on essentially every collision.

Even in the absence of complete information about the pyrazine product states, the $P(\Delta E)$ curve shown in Figure 7 yields useful information about the V−RT pathway. The low-energy side of $P(\Delta E)$ begins at ΔE of approximately −500 cm^{-1} and extends to ~3000 cm^{-1}, with 95% of the energy transfer collisions occurring with ΔE < 1800 cm^{-1}. $P(\Delta E)$ is negligible for ΔE > 3000 cm^{-1} indicating that the probability of two-quanta transitions involving the high-frequency C−H stretch modes is low. Energy transfer with ΔE < 3000 cm^{-1} can occur either through single or multiquanta transitions from hot pyrazine. However, the $P(\Delta E)$ distribution is a smooth function of ΔE and shows no resonant features at the energies of pyrazine's vibrations. This indicates that combinations of vibrational modes are most likely involved in the observed energy transfer. This is reasonable given that pyrazine has a

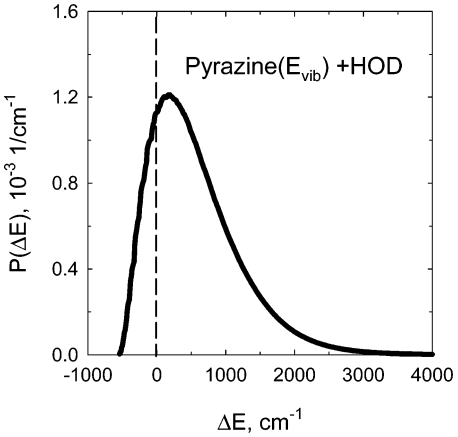

Figure 7. Energy transfer probability distribution function, $P(\Delta E)$, for collisions between highly vibrationally excited pyrazine and HOD.

near continuum of vibrational states with a high state density ($\rho \sim 5 \times 10^{13}$ cm^{-1}). The $P(\Delta E)$ distribution peaks at $\Delta E =$ 170 cm^{-1} rather than at $\Delta E = 0$ as expected from propensity rules that favor energy transfer for minimum values of ΔE. This shift may correspond to the changes in pyrazine rotational energy or our choice of initial energy of the collision partners. The integrated probability has a value of $P_{int} = 1.7$ rather than unity since the Lennard-Jones collision rate is used as a reference in eq 7. From $P(\Delta E)$ we find that $\langle \Delta E_{down} \rangle = -57$ cm^{-1} and $\langle \Delta E_{up} \rangle = 975$ cm^{-1} with an overall $\langle \Delta E \rangle = 918$ cm^{-1}. If the experimentally determined collision rate is used in eq 7 instead of the Lennard-Jones collision rate, the average energy transfer values from $P(\Delta E)$ are $\langle \Delta E_{down} \rangle = -34$ cm^{-1} and $\langle \Delta E_{up} \rangle = 588$ cm^{-1} with an overall $\langle \Delta E \rangle = 554$ cm^{-1}. Thus, V−RT energy transfer from pyrazine (E_{vib}) to HOD(000) occurs with ΔE values that are relatively small and with probabilities that exceed the Lennard-Jones collision rate. The overall result is that V−RT energy transfer is dominated by small ΔE transitions that occur on nearly every collision (Figure 6). Whether this is a general mechanism for quenching of vibrationally hot molecules with polar baths remains to be seen.

Although average energy transfer values have not been reported previously for pyrazine (E_{vib})/HOD collisions, our results are of the same order of magnitude as the values reported by Miller and Barker.[22] They find that quenching collisions of highly excited donors with polar bath molecules such as water and ammonia are generally more efficient than quenching with nonpolar bath species of comparable size. They report $\langle \Delta E \rangle =$ 475 cm^{-1} for the quenching of pyrazine ($E_{vib} = 24\,000$ cm^{-1}) with NH_3, so we can anticipate a similar value for quenching in water. When CO_2 and CH_4 are the bath species, the values are smaller with $\langle \Delta E \rangle \sim 180$ cm^{-1}. Our results show that the collision rate of pyrazine with HOD is nearly twice that of the Lennard-Jones collision rate. Therefore, it is likely that the average energy transfer value for pyrazine with NH_3 is closer to 250−300 cm^{-1}. This range of values is still greater than those for CO_2. It is well documented from state-resolved studies that the quenching of pyrazine (E_{vib}) with CO_2 has a prominent strong collision tail with non-negligible probability for ΔE values as large as 8000 cm^{-1}.[44,49,61] On the basis of the average value of ΔE measured by Miller and Barker and the supercollision tail for pyrazine/CO_2, there must exist an intense feature in $P(\Delta E)$ at low ΔE values due to weak collisions with CO_2 and pyrazine. We can therefore conclude that the shape of $P(\Delta E)$ for quenching in CO_2 is substantially different than that reported here for quenching in HOD. This conclusion underscores the fact that direct measurements of $P(\Delta E)$ can provide significantly more information about energy transfer processes than can the average energy transfer values. It will be important to apply our technology to measure weak collisions for other bath species in order to develop a more complete understanding of the role of strong and weak collisions in quenching high-energy molecules.

Conclusion

This work describes state-resolved measurements of energy gain in HOD(000) that results from weak and strong collisions of HOD with highly vibrationally excited pyrazine. Information about weak collisional energy transfer is extracted from Doppler-broadened transient line profiles for low-J states of HOD. Scattered HOD molecules in low- and high-J states are described by a single Boltzmann distribution. The integrated energy transfer rate for the V−RT pathway is larger than the Lennard-Jones collision rate by a factor of 1.7. We estimate that the V−RT pathway accounts for ∼95% of all collisions between pyrazine (E_{vib}) and HOD. The translational energy of the scattered HOD molecules increases slightly as a function of HOD rotational energy, as expected for impulsive energy transfer. Depletion measurements for low-J states show that the initial HOD has translational energy profiles that are close to 300 K. It remains to be seen if the dynamics of the depletion process will be similar for different collision systems. The distribution for energy gain, $P(\Delta E)$, shows that 95% of V−RT quenching collisions between with HOD and pyrazine (E_{vib}) occur with ΔE values less than 1800 cm^{-1}. These results provide a nearly complete picture of how energy is partitioned in collisions of highly excited molecules with molecular collision partners. The ability to measure weak collisions is an important step toward the development of a more predictive understanding of the detailed features that underlie collisional energy transfer in highly excited molecules and of how internal energy affects these processes.

Acknowledgment. The work at Boston University and the University of Maryland was supported by the NSF (Grants 0316836 and 0552663) with additional equipment provided by the DOE (DE-FG02-06ER15761).

References and Notes

(1) Roehl, C. M.; Nizkorodov, S. A.; Zhang, H.; Blake, G. A.; Wennberg, P. O. *J. Phys. Chem. A* **2002**, *106*, 3766−3772.
(2) Feierabend, K. J.; Havey, D. K.; Brown, S. S.; Vaida, V. *Chem. Phys. Lett.* **2006**, *420*, 438−442.
(3) Vaida, V.; Kjaergaard, H. G.; Hintze, P. E.; Donaldson, D. J. *Science* **2003**, *299*, 1566−1568.
(4) Brown, S. S.; Wilson, R. W.; Ravishankara, A. R. *J. Phys. Chem. A* **2000**, *104*, 4976−4983.
(5) Bailey, A. E.; Heard, D. E.; Henderson, D. A.; Paul, P. H. *Chem. Phys. Lett.* **1999**, *302*, 132−138.
(6) Bailey, A. E.; Heard, D. E.; Paul, P. H.; Pilling, M. J. *J. Chem. Soc., Faraday Trans.* **1997**, *93*, 2915−2920.
(7) Heidner, R. F.; Husain, D.; Wiesenfeld, J. R. *J. Chem. Soc., Faraday Trans. 2* **1973**, *69*, 927−938.
(8) Filseth, S. V.; Zia, A.; Welge, K. H. *J. Chem. Phys.* **1970**, *52*, 5502.
(9) Clark, I. D.; Wayne, R. P. *Proc. R. Soc. London, Ser. A* **1969**, *314*, 111.
(10) Drake, M. C.; Ratcliffe, J. W. *J. Chem. Phys.* **1993**, *98*, 3850−3865.
(11) Paul, P. H.; Gray, J. A.; Durant, J. L.; Thoman, J. W. *Appl. Phys. B* **1993**, *57*, 249−259.
(12) Paul, P. H.; Gray, J. A.; Durant, J. L.; Thoman, J. W. *AIAA J.* **1994**, *32*, 1670−1675.
(13) Tamura, M.; Berg, P. A.; Harrington, J. E.; Luque, J.; Jeffries, J. B.; Smith, G. P.; Crosley, D. R. *Combust. Flame* **1998**, *114*, 502−514.
(14) Smyth, K. C. *Combust. Sci. Technol.* **1996**, *115*, 151−176.
(15) Miller, J. A.; Klippenstein, S. J. *J. Phys. Chem. A* **2006**, *110*, 10528−10544.

(16) Fernandez-Ramos, A.; Miller, J. A.; Klippenstein, S. J.; Truhlar, D. G. *Chem. Rev.* **2006**, *106*, 4518−4584.
(17) Havey, D. K.; Liu, Q.; Li, Z. M.; Elioff, M.; Fang, M.; Neudel, J.; Mullin, A. S. *J. Phys. Chem. A* **2007**, *111*, 2458−2460.
(18) Hippler, H.; Troe, J.; Wendelken, H. J. *Chem. Phys. Lett.* **1981**, *84*, 257−259.
(19) Toselli, B. M.; Brenner, J. D.; Yerram, M. L.; Chin, W. E.; King, K. D.; Barker, J. R. *J. Chem. Phys.* **1991**, *95*, 176−188.
(20) Toselli, B. M.; Barker, J. R. *J. Chem. Phys.* **1991**, *95*, 8108−8119.
(21) Toselli, B. M.; Barker, J. R. *J. Chem. Phys.* **1992**, *97*, 1809−1817.
(22) Miller, L. A.; Barker, J. R. *J. Chem. Phys.* **1996**, *105*, 1383−1391.
(23) Brenner, J. D.; Erinjeri, J. P.; Barker, J. R. *Chem. Phys.* **1993**, *175*, 99−111.
(24) Miller, L. A.; Cook, C. D.; Barker, J. R. *J. Chem. Phys.* **1996**, *105*, 3012−3018.
(25) Smith, G. P.; Barker, J. R. *Chem. Phys. Lett.* **1981**, *78*, 253−258.
(26) Hold, U.; Lenzer, T.; Luther, K.; Reihs, K.; Symonds, A. C. *J. Chem. Phys.* **2000**, *112*, 4076−4089.
(27) Lenzer, T.; Luther, K.; Reihs, K.; Symonds, A. C. *J. Chem. Phys.* **2000**, *112*, 4090−4110.
(28) Grigoleit, U.; Lenzer, T.; Luther, K.; Mutzel, M.; Takahara, A. *Phys. Chem. Chem. Phys.* **2001**, *3*, 2191−2202.
(29) Hold, U.; Lenzer, T.; Luther, K.; Symonds, A. C. *J. Chem. Phys.* **2003**, *119*, 11192−11211.
(30) Frerichs, H.; Lenzer, T.; Luther, K.; Schwarzer, D. *Phys. Chem. Chem. Phys.* **2005**, *7*, 620−626.
(31) Frerichs, H.; Hollerbach, M.; Lenzer, T.; Luther, K. *J. Phys. Chem. A* **2006**, *110*, 3179−3185.
(32) Ma, J. Q.; Liu, P.; Zhang, M.; Dai, H. L. *J. Chem. Phys.* **2005**, *123*, 154306.
(33) Qin, D.; Hartland, G. V.; Chen, C. L.; Dai, H. L. *Z. Phys. Chem.* **2000**, *214*, 1501−1519.
(34) Letendre, L. T.; McNavage, W.; Pibel, C.; Liu, D. K.; Dai, H. L. *J. Chin. Chem. Soc.* **2005**, *52*, 677−686.
(35) Kreutz, T. G.; Oneill, J. A.; Flynn, G. W. *J. Phys. Chem.* **1987**, *91*, 5540−5543.
(36) Sedlacek, A. J.; Weston, R. E.; Flynn, G. W. *J. Chem. Phys.* **1991**, *94*, 6483−6490.
(37) Flynn, G. W.; Weston, R. E. *J. Phys. Chem.* **1993**, *97*, 8116−8127.
(38) Fraelich, M.; Elioff, M. S.; Mullin, A. S. *J. Phys. Chem. A* **1998**, *102*, 9761−9771.
(39) Elioff, M. S.; Fang, M.; Mullin, A. S. *J. Chem. Phys.* **2001**, *115*, 6990−7001.
(40) Liu, Q. N.; Du, J.; Havey, D. K.; Li, Z. M.; Miller, E. M.; Mullin, A. S. *J. Phys. Chem. A* **2007**, *111*, 4073−4080.
(41) Weston, R. E., Jr.; Flynn, G. W. *Annu. Rev. Phys. Chem.* **1992**, *43*, 559−589.
(42) Flynn, G. W.; Weston, R. E., Jr. *J. Phys. Chem.* **1993**, *97*, 8116−8127.
(43) Sedlacek, A. J.; Weston, R. E., Jr.; Flynn, G. W. *J. Chem. Phys.* **1991**, *94*, 6483−6490.
(44) Mullin, A. S.; Park, J.; Chou, J. Z.; Flynn, G. W.; Weston, R. E., Jr. *Chem. Phys.* **1993**, *175*, 53−70.
(45) Michaels, C. A.; Mullin, A. S.; Flynn, G. W. *J. Chem. Phys.* **1995**, *102*, 6682−6695.
(46) Mullin, A. S.; Michaels, C. A.; Flynn, G. W. *J. Chem. Phys.* **1995**, *102*, 6032−6045.
(47) Michaels, C. A.; Lin, Z.; Mullin, A. S.; Tapalian, H. C.; Flynn, G. W. *J. Chem. Phys.* **1997**, *106*, 7055−7071.
(48) Sevy, E. T.; Rubin, S. M.; Lin, Z.; Flynn, G. W. *J. Chem. Phys.* **2000**, *113*, 4912−4932.
(49) Wall, M. C.; Mullin, A. S. *J. Chem. Phys.* **1998**, *108*, 9658−9667.
(50) Wall, M. C.; Stewart, B. A.; Mullin, A. S. *J. Chem. Phys.* **1998**, *108*, 6185−6196.
(51) Park, J.; Shum, L.; Lemoff, A. S.; Werner, K.; Mullin, A. S. *J. Chem. Phys.* **2002**, *117*, 5221−5233.
(52) Miller, E. M.; Murat, L.; Bennette, N.; Hayes, M.; Mullin, A. S. *J. Phys. Chem. A* **2006**, *110*, 3266−3272.
(53) Elioff, M. S.; Sansom, R. L.; Mullin, A. S. *J. Phys. Chem. A* **2000**, *104*, 10304−10311.
(54) Elioff, M. S.; Fraelich, M.; Sansom, R. L.; Mullin, A. S. *J. Chem. Phys.* **1999**, *111*, 3517−3525.
(55) Elioff, M. S.; Fang, M.; Mullin, A. S. *J. Chem. Phys.* **2001**, *115*, 6990−7001.
(56) Li, Z.; Korobkova, E.; Werner, K.; Shum, L.; Mullin, A. S. *J. Chem. Phys.* **2005**, *123*, 174306/174301−174306/174309.
(57) Sushida, K.; Fujita, M.; Yamazaki, I.; Baba, H. *Bull. Chem. Soc. Jpn.* **1983**, *56*, 2228−2233.
(58) Yamazaki, I.; Murao, T.; Yoshihara, K.; Fujita, M.; Sushida, K.; Baba, H. *Chem. Phys. Lett.* **1982**, *92*, 421−424.
(59) Nelson, D. D., Jr.; Schiffman, A.; Lykke, K. R.; Nesbitt, D. J. *Chem. Phys. Lett.* **1988**, *153*, 105−111.
(60) Pyper, J. W.; Christensen, L. D. *J. Chem. Phys.* **1975**, *62*, 2596−2599.
(61) Wall, M. C.; Lemoff, A. S.; Mullin, A. S. *J. Phys. Chem. A* **1998**, *102*, 9101−9105.
(62) Lim, K. F. *Quantum Chem. Program Exch. Bull.* **1994**, *14*, 3.
(63) Michaels, C. A.; Flynn, G. W. *J. Chem. Phys.* **1997**, *106*, 3558−3566.